

**Oxygen reduction activity on perovskite oxide  
surfaces:  
a comparative first-principle study of  $\text{LaMnO}_3$ ,  
 $\text{LaFeO}_3$  and  $\text{LaCrO}_3$**

Yan Wang and Hai-Ping Cheng\*

*Department of Physics and Quantum Theory Project, University of Florida, Gainesville, Florida  
32611, USA*

E-mail: hping@ufl.edu

---

\*To whom correspondence should be addressed

## Abstract

The understanding of oxygen reduction reaction (ORR) activity on perovskite oxide surfaces is essential for promising future fuel cell applications. We report a comparative study of ORR mechanisms on  $\text{LaBO}_3$  ( $B=\text{Mn, Fe, Cr}$ ) surfaces by first-principles calculations based on density functional theory (DFT). Results obtained from varied DFT methods such as generalized gradient approximation (GGA), GGA+ $U$  and the hybrid Hartree-Fock density functional method are reported for comparative purposes. We find that the results calculated from hybrid-functional method suggest that the order of ORR activity is  $\text{LaMnO}_3 > \text{LaCrO}_3 > \text{LaFeO}_3$ , which is in better agreement with recent experimental results (Suntivich *et al.*, Nature Chemistry 3, 546 (2011)) than those using the GGA or GGA+ $U$  method.

# INTRODUCTION

Oxygen reduction reaction (ORR), one of electrochemical energy conversion processes, plays a very important role in renewable energy technologies, including fuel cells and metal-air batteries. Searching for a highly active catalyst to replace noble metal cathodes is driven by the need of efficient and low-cost ORR catalysts, which are essential for mass marketing a fuel cell technology to address the world's energy needs.

Recent experiments by Suntivich *et al.*<sup>1,2</sup> shows that perovskite transition-metal oxides can exhibit high electrocatalytic activity for ORR in alkaline electrolytes. It is also suggested that ORR activity on perovskite oxide surfaces is related to the  $e_g$  occupation in the  $B$ -site cation, which is indicative of the strength of bonding between transition metal ion and adsorbed oxygen. A moderate amount of  $e_g$ -filling in perovskite oxides such as  $\text{LaMnO}_3$  ( $e_g = 1$ ) yields higher activity as compared to other oxides with either too little ( $\text{LaCrO}_3$  with  $e_g = 0$ ) or too much  $e_g$  electron filling ( $\text{LaFeO}_3$  with  $e_g = 2$ ).

ORR on  $\text{LaBO}_3$  perovskite oxide surfaces has been theoretically investigated extensively in the past using first-principles methods based on density functional theory.<sup>3-8</sup> All of these studies considered atomic and molecular oxygen adsorption on the  $\text{LaBO}_3$  surface only for its application in solid oxide fuel cells. However, in alkaline fuel cells the ORR involves a more complicated reaction pathway, in which ORR intermediates such as hydroxides and peroxides<sup>2</sup> will form on the surface. Furthermore, in most studies the standard (semi) local DFT methods, local density approximation or generalized gradient approximation (GGA), are used, while only a few of them use GGA+ $U$  approach to describe strongly correlated electrons.<sup>8,9</sup> The role of GGA+ $U$  is to address on-site Coulomb interactions in the localized orbitals (such as  $d$  orbitals in transition metals) with an additional Hubbard-type term  $U$ .<sup>10,11</sup> It has been found that  $\text{LaBO}_3$  surface energetics are strongly depend on the parameter  $U$  used in the calculation.<sup>8</sup>

These recent studies further motivate us to use higher-level theoretical treatments, the so-called "parameter-free" hybrid functional approach, for a complete description of the ORR on the  $\text{LaBO}_3$  perovskite oxide surfaces. A hybrid functional, a combination of exact nonlocal orbital-dependent

Hartree-Fock exchange and a standard local exchange-correlation functional, provides a significant improvement over the GGA description and enables accurate computation of electronic properties and energetics of molecular systems as well as extended systems including transition metal oxides<sup>12-14</sup> without the need for system-dependent adjustable parameters or decisions of which electrons to localize. So far ORR activity on perovskite oxide surfaces is unexplored by hybrid-functional approaches. In the present work we aim at filling this gap.

In this paper we report a comparative study of ORR activity on  $\text{LaBO}_3$  ( $B=\text{Mn, Fe, Cr}$ ) perovskite oxide surfaces using first-principles calculations. Calculations based on various DFT functionals such as GGA, GGA+ $U$  and hybrid functional are performed for comparative purposes. From binding energies of ORR intermediates, we obtain free energy changes at each step of the ORR and present overall free energy diagrams for each surface. The kinetics of ORR on each perovskite oxide surface are found to differ significantly with different DFT methods used in the calculation. We find that the hybrid functional method yields better agreement with recent experiments by Suntivich *et al.*<sup>1,2</sup> while the results from the GGA and GGA+ $U$  methods fail to explain the experimental observations.

## Computational Methods

### DFT calculations

Our calculations are performed using the plane-wave-basis-set Vienna *ab initio* simulation package VASP<sup>15</sup> (version 5.2). The projector-augmented-wave (PAW) methods are used to describe the interactions between atomic cores and valence electrons, with a kinetic energy cutoff of 500 eV employed in all simulations. The  $3p$ -semi-core states are treated as valence states for transition metal atoms Cr ( $3p^6 3d^5 4s^1$ ), Mn ( $3p^6 3d^5 4s^2$ ), and Fe ( $3p^6 3d^6 4s^2$ ). For the exchange-correlation functional we used the GGA method with Perdew-Burke-Ernzerhof (PBE) formulation.<sup>16</sup> We also apply the GGA+ $U$  method to reduce the self-interaction error and improve the description of correlation effects. For the GGA+ $U$  calculation we make use of the standard Dudarev implementation<sup>17</sup>

where the on-site Coulomb interaction for the localized orbitals is parametrized by  $U_{\text{eff}} = U - J$  using the PBE functional. We apply the optimized effective interaction parameter  $U_{\text{eff}}$  for the metal atoms in  $\text{LaBO}_3$  ( $U_{\text{eff}} = 4, 4$  and  $3.5$  eV for Mn, Fe and Cr, respectively), determined by fitting the enthalpies of the oxidation reactions.<sup>18</sup> These values have previously been shown to provide a description of  $\text{LaBO}_3$  electronic structure that is in good agreement with the available experimental data.<sup>8</sup> Furthermore, we perform single-point total energy calculations with the hybrid functional approach developed by Heyd-Scuseria-Ernzerhof (HSE06)<sup>19</sup> for the approximation of the exchange-correlation energy and potential. In the HSE06 approach, one quarter of the PBE short-range exchange is replaced by the exact Hartree-Fock exchange, and the full PBE correlation energy is included. The range-separation parameter is set to be  $0.2 \text{ \AA}^{-1}$ .

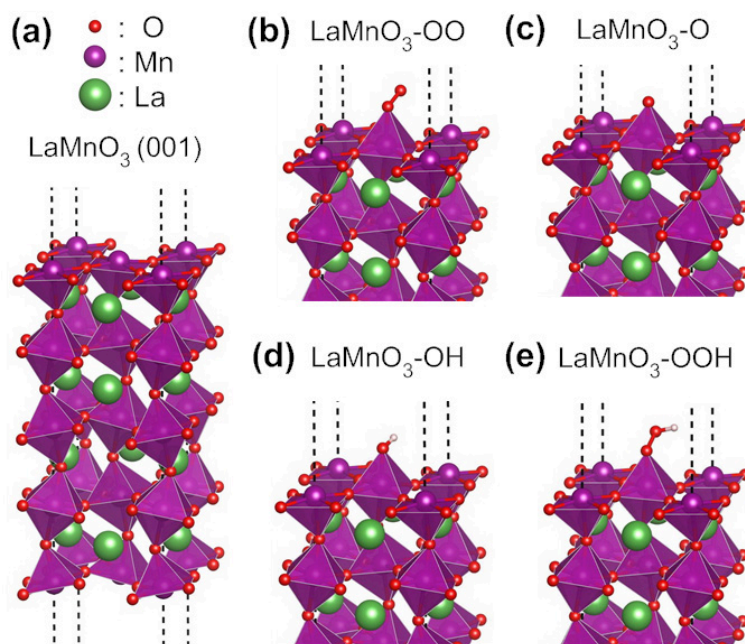


Figure 1: (Color online). Optimized geometry of bare  $\text{LaMnO}_3$  (001) surface (a) and surfaces with adsorbed ORR intermediates  $\text{OO}^*$  (b),  $\text{O}^*$  (c),  $\text{HO}^*$  (d), and  $\text{HOO}^*$  (e) intermediates. The dashed lines are the boundaries of the supercell.

The  $\text{LaBO}_3$  perovskite oxide surfaces are simulated with a slab including nine atomic layers with transition metal  $B$ -terminated (001) surfaces at each side. Such surfaces are chosen simply because the (001) surfaces are generally the most stable in perovskites and the redox active transition metal atoms are expected to be responsible for ORR catalytic activity.<sup>2</sup> The distorted perovskite

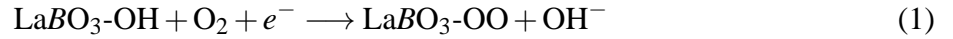
structure of *pnma* is considered to be the structure identified in the experiment of Ref. (author?)<sup>2</sup>, and the equilibrium bulk geometry with optimized lattice constants is used to construct the  $\text{LaBO}_3$  slab geometries. A large vacuum spacing of  $15 \text{ \AA}$  was used between two slabs to prevent interaction between the system with its images in adjacent unit cells. We use the  $1 \times 1$  surface unit cell, and two-dimensional periodic boundary conditions are applied for the surface directions with a  $6 \times 6$  Monkhorst-Pack type of  $k$ -point sampling.<sup>20</sup> The four bottom atomic layers of the slab are fixed at the optimized bulk lattice constant, while the top five layers as well as the ORR intermediate on the surface are fully relaxed. In all calculations a dipole correction is applied. The ORR intermediates are modeled by the same slab with the intermediate adsorbed at the  $B$  sites on the top surface of the slab. Adsorbates placed above the surfaces correspond to a coverage of 50%. The geometries are optimized until the force on each atom falls below the convergence criterion of  $0.02 \text{ eV/\AA}$ . The optimized structures of bare  $\text{LaBO}_3$  surfaces and surfaces with adsorbed ORR intermediates  $\text{OO}^*$ ,  $\text{O}^*$ ,  $\text{HO}^*$  and  $\text{HOO}^*$  (asterisk denoting adsorbed species hereafter), taking  $\text{LaMnO}_3$  as an example, are shown in Fig. 1 (a)-(e). For the HSE06 calculations, four bottom atomic layers of each  $\text{LaBO}_3$  slab are removed in order to save computational effort.

The magnetic structures of  $\text{LaBO}_3$  perovskites are complicated due to phase transitions at different temperatures. For simplicity and consistency we apply the ferromagnetic ordering for all the studied  $\text{LaBO}_3$  perovskites, by an initial assignment of non-zero (parallel) spin to all the  $B$  atoms. The self-consistent procedure determining the electron and spin density distribution for each geometry are always carried out leaving the total spin unconstrained and free to evolve. We expect our assumption will not introduce large errors in our energetic results, as we focus on the adsorption energy and relative free energy of the ORR intermediates on the surface, in which the total energy difference caused by changing the relative spin orientations inside the slab should have negligible effect.

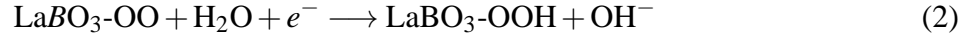
## Free energy diagrams for oxygen reduction reaction

The following four-electron ORR reaction pathway for  $\text{LaBO}_3$  at the cathode in alkaline electrolytes has been suggested<sup>2</sup> (overall process  $\text{O}_2 + 2\text{H}_2\text{O} + 4e^- \rightarrow 4\text{OH}^-$ ):

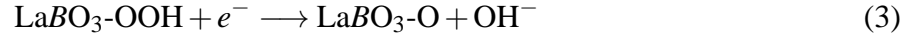
1) surface hydroxide displacement as:



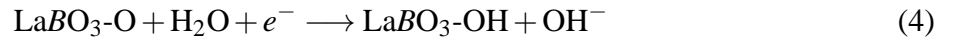
2) surface peroxide formation as:



3) surface oxide formation as:



and 4) surface hydroxide regeneration as:



The free energy change of each ORR reaction step is calculated based on a computational hydrogen electrode model suggested by Nørskov *et al.*<sup>21</sup> This method has been shown to predict trends for the oxygen reduction reaction on metals quite well.<sup>21</sup> In this method the potential affects the relative free energy through the chemical potential of the electrons in the electrode. We convert the calculated DFT energies into Gibbs free energies by adding entropic ( $T\Delta S$ ) and zero-point energy (ZPE) corrections to the ORR intermediates, so that

$$\Delta G = \Delta E + \Delta \text{ZPE} - T\Delta S + \Delta G_\Phi \quad (5)$$

where  $\Delta E$  is the calculated DFT reaction energy,  $\Delta ZPE$  is the change in ZPE and  $\Delta S$  is the change in the entropy. ZPE corrections and entropies of the ORR intermediates are calculated from the vibrational frequencies according to standard methods, and those of the gas-phase molecules are obtained from thermodynamics databases.  $\Delta G_\Phi$  is the effect of electrode potential which is applied by shifting the free energy change  $\Delta G$  by  $\Delta G_\Phi = e\Phi$ , where  $e$  is the elementary charge and  $\Phi$  is the potential difference between electrode and counter electrode (versus reversible hydrogen electrode, RHE). The equilibrium potential  $\Phi_{\text{eq}}$  corresponds to zero net reaction free energy ( $\sum_{i=1}^4 G_i = 2\Delta G_W + 4e\Phi = 0$ ) of the overall ORR process, thus we have  $\Phi_{\text{eq}} = -\Delta G_W/(2e)$ , where  $\Delta G_W = G(\text{H}_2\text{O}) - G(\text{H}_2) - G(\text{O}_2)/2$  is the free energy of formation of water from  $\text{H}_2$  and  $\frac{1}{2}\text{O}_2$ . The ORR potential  $\Phi_{\text{ORR}}$  corresponds to the highest potential  $\Phi$  at which all steps along the reaction decrease the free energy. The theoretical ORR overpotential is then calculated by  $\eta = \Phi_{\text{eq}} - \Phi_{\text{ORR}}$ .

Furthermore, effect of water on the ORR activity is also taken into account by a solvation correction to ORR intermediates, since reactions occur in the presence of water in electrolytes.<sup>2</sup> The solvation corrections are obtained from a previous study of platinum-catalyzed ORR using the Poisson-Boltzmann implicit continuum model.<sup>22</sup> The solvation correction energies are  $-0.32$ ,  $-0.47$ ,  $-0.75$  and  $-0.54$  eV for  $\text{OO}^*$ ,  $\text{O}^*$ ,  $\text{HO}^*$ , and  $\text{HOO}^*$  intermediates, respectively.

## Results and discussion

### Surface Energetics and Electronic properties

We first calculate the DFT binding energy for each ORR intermediate on the  $\text{LaBO}_3$  (001) surfaces. The DFT binding energies of the ORR intermediates are calculated according to  $\Delta E_{\text{adsorbate}} = E_{\text{LaBO}_3\text{-adsorbate}} - E_{\text{LaBO}_3} - E_{\text{adsorbate}}$ , where  $E_{\text{LaBO}_3\text{-adsorbate}}$ ,  $E_{\text{LaBO}_3}$  and  $E_{\text{adsorbate}}$  are the energies of the surface with adsorbed intermediate, the bare surface and the isolated ORR intermediate, respectively. The negative sign of  $E_{\text{adsorbate}}$  corresponds to energy gain of the system due to adsorption of ORR intermediate, and the more negative the  $E_{\text{adsorbate}}$  value the stronger is the chemical



**Table 1: Calculated DFT binding energy of each ORR intermediate on  $\text{LaBO}_3$  surfaces (unit: eV). The DFT binding energies of the ORR intermediates are calculated according to  $\Delta E_{\text{adsorbate}} = E_{\text{LaBO}_3\text{-adsorbate}} - E_{\text{LaBO}_3} - E_{\text{adsorbate}}$ . The absorption energies  $\Delta E_{\text{adsorbate}}^{\text{ad}}$  relative to energies of  $\text{H}_2\text{O}$  and  $\text{H}_2$  are also given (in parentheses, see text for definition).**

structures	method	$\Delta E_{\text{OH}} (\Delta E_{\text{OH}}^{\text{ad}})$	$\Delta E_{\text{OO}}$	$\Delta E_{\text{OOH}} (\Delta E_{\text{OOH}}^{\text{ad}})$	$\Delta E_{\text{O}} (\Delta E_{\text{O}}^{\text{ad}})$
LaMnO <sub>3</sub>	GGA	-2.927 (0.417)	-0.659	-1.424 (3.739)	-3.755 (1.913)
	GGA+ <i>U</i>	-2.107 (1.236)	-0.205	-0.724 (4.439)	-1.987 (3.681)
	HSE06	-1.647 (1.355)	0.162	-0.482 (4.844)	-1.278 (4.015)
LaFeO <sub>3</sub>	GGA	-2.686 (0.658)	-0.491	-1.224 (3.939)	-3.457 (2.211)
	GGA+ <i>U</i>	-2.287 (1.057)	-0.199	-0.794 (4.369)	-2.134 (3.534)
	HSE06	-1.778 (1.223)	0.328	-0.028 (5.298)	-1.368 (3.926)
LaCrO <sub>3</sub>	GGA	-3.276 (0.068)	-0.931	-1.786 (3.377)	-4.986 (0.682)
	GGA+ <i>U</i>	-2.429 (0.915)	-0.172	-1.014 (4.149)	-3.515 (2.153)
	HSE06	-1.858 (1.144)	0.305	-0.678 (4.648)	-2.972 (2.322)

interaction between the adsorbate and the surface. It should be also noted that our calculations give the reference energies of  $-9.86$  and  $-17.04$  eV for  $\text{O}_2$  with the GGA and the hybrid functional, respectively, and no correction for this has been made in the values of this work. While such a correction would alter the absolute binding energies it has no effect on the relative difference in binding energies between surfaces. The results are summarized in Table 1 for comparison among different DFT functionals. It is clear that for each ORR intermediate the binding energy (absolute values) decreases from the GGA value to that of GGA+*U* and then especially strongly to the HSE06 hybrid-functional result. This holds for all three perovskite surfaces.

Among the four ORR intermediates, the  $\text{O}^*$  binding energy has the strongest dependence of the calculating method. Taking LaMnO<sub>3</sub> as an example, the GGA binding energy  $E_{\text{O}}$  is about 1.8 eV larger (in its absolute value) than that of GGA+*U*, and it is about 2.5 eV larger than the HSE06 value. For the binding energy  $E_{\text{OO}}$  a relatively weaker dependence can be found. For LaMnO<sub>3</sub> the difference between calculated values of  $E_{\text{OO}}$  from the GGA and GGA+*U* methods is about 0.45 eV, and that between the GGA and HSE06 methods is about 0.8 eV. Similar behaviors can be also found for LaFeO<sub>3</sub> and LaCrO<sub>3</sub> in Table 1. These can be explained by the fact that the interaction between atomic oxygen and the surface transition metal *B* ion is much stronger than the other ORR intermediates, thus the effect of correlation corrections in the the GGA+*U* and

HSE06 calculations are much more obvious on the O\* binding energies. The calculated charge transfer results further support this point. In Table 2 we show the effective Bader charges (based on the real-space-charge density<sup>23</sup>) of transition metal ion and adsorbed ORR intermediate on each LaBO<sub>3</sub> surface. It is clear that the charge transfer between the surface and the adsorbed ORR intermediate is large for LaBO<sub>3</sub>-O but much smaller for LaBO<sub>3</sub>-OO. Our results are consistent with a recent *ab initio* GGA+*U* study by Lee *et al.*,<sup>8</sup> which also shows that the O\* binding on the LaBO<sub>3</sub> surface has a stronger  $U_{\text{eff}}$  dependence than the OO\* binding. In our calculations, the even larger correction of binding energies in the HSE06 hybrid functional results compared to the corrections in the results from the GGA+*U* method is primarily due to the fact that the  $U_{\text{eff}}$  is applied only at the transition metal *B* atoms in the GGA+*U* calculations.

**Table 2: Effective Bader charges  $q$  (in  $e$ ) of transition metal ions and adsorbed ORR intermediates (in parentheses) on LaBO<sub>3</sub> surfaces.**

perovskites	method	bare surface	LaBO <sub>3</sub> -OO	LaBO <sub>3</sub> -OOH	LaBO <sub>3</sub> -O	LaBO <sub>3</sub> -OH
LaMnO <sub>3</sub>	GGA	1.66	1.78 (-0.31)	1.81 (-0.36)	1.80 (-0.51)	1.82 (-0.39)
	GGA+ <i>U</i>	1.71	1.76 (-0.16)	1.81 (-0.30)	1.86 (-0.52)	1.89 (-0.44)
	HSE06	1.83	1.91 (-0.25)	1.96 (-0.37)	1.93 (-0.46)	1.99 (-0.42)
LaFeO <sub>3</sub>	GGA	1.57	1.64 (-0.24)	1.68 (-0.33)	1.70 (-0.52)	1.74 (-0.47)
	GGA+ <i>U</i>	1.79	1.84 (-0.15)	1.85 (-0.35)	1.73 (-0.54)	1.83 (-0.47)
	HSE06	1.81	1.94 (-0.18)	1.93 (-0.41)	1.87 (-0.57)	1.95 (-0.55)
LaCrO <sub>3</sub>	GGA	1.78	1.92 (-0.40)	1.91 (-0.39)	2.01 (-0.55)	1.93 (-0.42)
	GGA+ <i>U</i>	1.81	1.97 (-0.18)	1.93 (-0.29)	2.02 (-0.51)	1.99 (-0.39)
	HSE06	1.94	2.02 (-0.28)	1.91 (-0.39)	2.17 (-0.56)	2.14 (-0.43)

In comparing the calculated binding energies of the three LaBO<sub>3</sub> systems, we notice that for each ORR intermediate the binding energy (in its absolute value) is generally larger for LaCrO<sub>3</sub> than that of LaMnO<sub>3</sub> or LaFeO<sub>3</sub>, with the only exception the OO\* intermediate with the GGA+*U* and HSE06 results. In particular, the binding energy  $E_{\text{O}}$  for LaCrO<sub>3</sub> is (depending on the method) about 1.2~1.7 and 1.4~1.6 eV more negative than that of LaMnO<sub>3</sub> and LaFeO<sub>3</sub>, respectively, indicating a stronger interaction between the LaCrO<sub>3</sub> surface and the atomic oxygen adsorbate. For the OO\* intermediate, we find that though the GGA results still show a  $\sim 0.3$  eV larger binding energy (in its absolute value) for LaCrO<sub>3</sub> as compared to the LaMnO<sub>3</sub> ( $\sim 0.4$  eV larger as compared to LaFeO<sub>3</sub>), the GGA+*U* method yields very similar binding energies of molecular oxygen for all

three perovskite surfaces. The HSE06 method, however, gives the largest binding energy  $E_{OO}$  with a positive sign for LaFeO<sub>3</sub> surface, indicating a relatively weak binding ability of LaFeO<sub>3</sub> surface for OO\* intermediate. This is also true for the HOO\* intermediate where the HSE06 method yields smaller binding energy  $E_{OOH}$  (in its absolute value) for LaFeO<sub>3</sub> than the other two perovskites.

In Table 1 we also show the calculated adsorption energies of HO\*, HOO\* and O\* intermediates relative to H<sub>2</sub>O and H<sub>2</sub>, according to the following reactions as defined in Ref. (author?)<sup>24</sup>:

$$\Delta E_{OH}^{ad} = E_{LaBO_3-OH} - E_{LaBO_3} - (E_{H_2O} - \frac{1}{2}E_{H_2}) \quad (6)$$

$$\Delta E_{OOH}^{ad} = E_{LaBO_3-OOH} - E_{LaBO_3} - (2E_{H_2O} - \frac{3}{2}E_{H_2}) \quad (7)$$

$$\Delta E_O^{ad} = E_{LaBO_3-O} - E_{LaBO_3} - (E_{H_2O} - E_{H_2}). \quad (8)$$

where  $E_{H_2O}$ , and  $E_{H_2}$  are the calculated energies of H<sub>2</sub>O and H<sub>2</sub> molecules in the gas phase, respectively. Our calculated adsorption energies of HO\*, HOO\* and O\* intermediates with the GGA-PBE method are very close to the recent reported results by Man *et al.*<sup>24</sup> using the GGA-RPBE method, with less than 0.1 eV difference for LaFeO<sub>3</sub> and LaCrO<sub>3</sub>. For LaMnO<sub>3</sub> our GGA adsorption energies are slightly larger than the results reported in Ref. (author?)<sup>24</sup>, with 0.55, 0.15 and 0.27 eV difference for the O\*, HO\* and HOO\* intermediates, respectively. The discrepancy may be because of different pseudopotentials (ultrasoft) used in the Ref. (author?)<sup>24</sup>.

### ORR on LaBO<sub>3</sub> surface

The calculated free energy change of each ORR step at zero electrode potential ( $\Phi = 0$  V vs. RHE) are listed in Table 3.  $\Delta G_1$ ,  $\Delta G_2$ ,  $\Delta G_3$ , and  $\Delta G_4$  correspond to the free energy changes in the ORR reaction steps of Eqs. (1), (2), (3) and (4), respectively. All reaction steps are exothermic for all three perovskite oxide surfaces with different calculation methods. However, for each surface GGA+*U* and HSE06 methods give quite different relations between different reaction steps respect

**Table 3: Calculated free energy change  $\Delta G$  for each ORR step in  $\text{LaBO}_3$  (unit: eV). \* denotes the potential-determining step for the ORR with the smallest  $|\Delta G|$ .**

structures	method	$\Delta G_1$	$\Delta G_2$	$\Delta G_3$	$\Delta G_4$
LaMnO <sub>3</sub>	GGA	-0.642*	-0.649*	-2.370	-1.000
	GGA+ <i>U</i>	-1.008	-0.403*	-1.302	-1.948
	HSE06	-0.758	-0.526*	-1.372	-2.165
LaFeO <sub>3</sub>	GGA	-0.715	-0.618*	-2.272	-1.057
	GGA+ <i>U</i>	-0.822	-0.479*	-1.379	-1.981
	HSE06	-0.462	-0.237*	-1.916	-2.206
LaCrO <sub>3</sub>	GGA	-0.564	-0.739	-3.239	-0.119*
	GGA+ <i>U</i>	-0.652*	-0.726	-2.540	-0.743
	HSE06	-0.405*	-0.864	-2.870	-0.682

to the GGA values. The size of the ORR potential-determining step can be estimated according to

$$G = \min(|\Delta G_1|, |\Delta G_2|, |\Delta G_3|, |\Delta G_4|). \quad (9)$$

In the following we further analyze the catalytic performance by calculating the free energy diagrams under equilibrium and ORR potentials for each  $\text{LaBO}_3$  surface.

Fig. 2 shows the free energy diagrams of the ORR on the  $\text{LaMnO}_3$  (001) surface with different calculation methods for representative potentials  $\Phi_{\text{eq}}$  and  $\Phi_{\text{ORR}}$ . At the equilibrium potential  $\Phi_{\text{eq}}$ , for the GGA method it is clear that only reaction step (3), surface  $\text{O}^*$  formation, are energetically downhill (exothermic) and all other three steps are uphill (endothermic). The  $\text{O}^*$  intermediate is stabilized on the  $\text{LaMnO}_3$  surface. This is very similar to the case of ORR on Pt(111) surfaces studied by Nørskov et al.<sup>21,25</sup> The first two steps of the ORR process, the surface  $\text{OO}^*/\text{HO}^*$  exchange and the  $\text{HOO}^*$  formation, are the two potential-determining steps. The fact that these two steps become exothermic at nearly the same ORR potential indicates that  $\text{LaMnO}_3$  has a reactivity close to optimal, as the free energy changes in the four reaction steps are linearly related; thus increasing one of the step will decrease another. The theoretical ORR overpotential is 0.52 V, which is very close to the theoretical overpotential of 0.48 V for ORR on Pt(111).<sup>25</sup> In contrast to the strongly bound  $\text{O}^*$  intermediate with the GGA functional, applying the GGA+*U* and HSE06 functionals change the results by giving much higher relative free energy of  $\text{O}^*$  intermediate in the

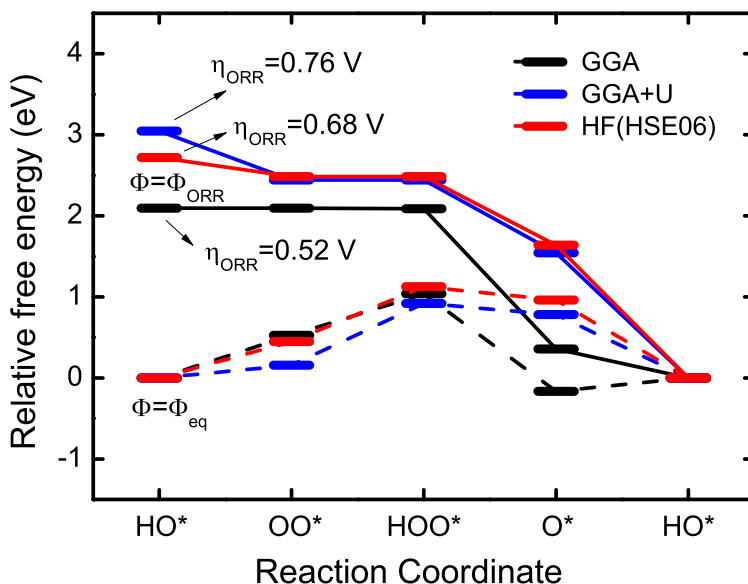


Figure 2: (Color online). Free energy diagrams of the ORR on the  $\text{LaMnO}_3$  (001) surface. Solid and dashed lines represent reactions at the ORR potential ( $\Phi = \Phi_{\text{ORR}}$ ) and the equilibrium potential ( $\Phi = \Phi_{\text{eq}}$ ), respectively. The ORR potential corresponds to the highest potential  $\Phi$  at which all steps along the reaction decrease the free energy. The theoretical overpotentials  $\eta$  are marked for results with different functionals.

ORR process. This should mainly be attributed to the largely decreased interaction strength between the  $\text{O}^*$  intermediate and the  $\text{LaMnO}_3$  surface for the GGA+ $U$  and HSE06 functionals with respect to the GGA result, consistent with the calculated binding energy as shown in Table 1. The  $\text{HO}^*$  intermediate becomes the most stable one on the  $\text{LaMnO}_3$  surface and the surface hydroxide regeneration (step 4) becomes exothermic. The potential limiting steps lie in the second electron transfer step of the ORR ( $\text{OOH}^*$  formation), and the theoretical ORR overpotentials are 0.76 V and 0.68 V for the GGA+ $U$  and HSE06 results, respectively.

The calculated free energy diagrams for ORR on the  $\text{LaFeO}_3$  (001) surface under  $\Phi_{\text{eq}}$  and  $\Phi_{\text{ORR}}$  are shown in Fig. 3. It has previously been suggested that for  $\text{LaFeO}_3$  the surface  $\text{OO}^*/\text{HO}^*$  exchange does not gain sufficient energy, and thus the ORR kinetics are limited by the rate of  $\text{OO}^*/\text{HO}^*$  exchange (step 1).<sup>2</sup> However, our calculation indicates that this reaction step is only the secondary potential-determining step. The primary potential-determining step is located at the  $\text{HOO}^*$  formation (step 2), which has a slightly larger free energy change than that of the  $\text{OO}^*/\text{HO}^*$  exchange step under equilibrium potential independent of the choice of the calculation method.

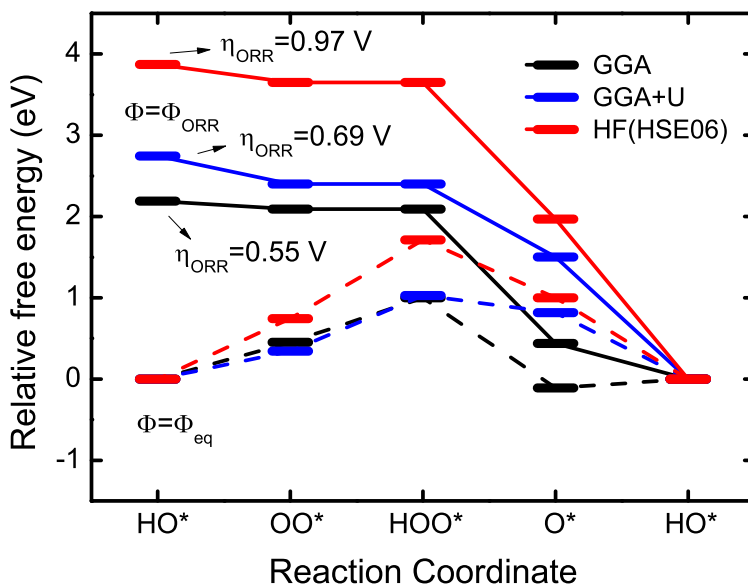


Figure 3: (Color online). Free energy diagrams of the ORR on the LaFeO<sub>3</sub> (001) surface.

The GGA calculation for LaFeO<sub>3</sub> yields results very similar to the calculated free energy diagram for LaMnO<sub>3</sub>, for which we obtain a low ORR overpotential of 0.55 V. Also similar to LaMnO<sub>3</sub>, the self-interaction corrections in the GGA+*U* and HSE06 calculations lower the binding energy of O\* on the LaFeO<sub>3</sub> surface and give clearly higher relative free energy for the O\* intermediate than the HO\* and OO\* intermediates in the ORR process. Moreover, for the HSE06 method the free energy change in the two endothermic steps, OO\*/HO\* exchange and HOO\* formation, are increased as compared to the results from GGA and GGA+*U*. As a result, while the GGA+*U* method gives a theoretical ORR overpotential of 0.69 V, comparable to the GGA method, the overpotential calculated for the HSE06 hybrid-functional is 0.97 V, which is almost twice as large as that of the GGA value.

For ORR on a LaCrO<sub>3</sub> (001) surface, at the equilibrium potential the O\* intermediate is strongly stabilized on the surface for the GGA functional, as shown in Fig. 4. This situation does not change much even if we apply the GGA+*U* method or HSE06 functional in the calculation. For the GGA functional it is clearly shown that the surface HO\* regeneration reaction (step 4) is the potential-determining step. The corresponding ORR overpotential is 1.05 V, much higher than that of LaMnO<sub>3</sub> or LaFeO<sub>3</sub>. This agrees very well with the experimental observations

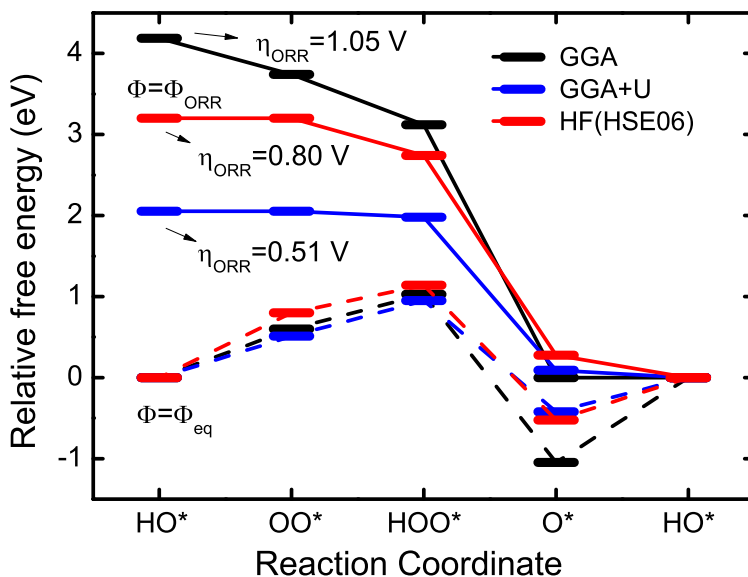


Figure 4: (Color online). Free energy diagrams of the ORR on the  $\text{LaCrO}_3$  (001) surface.

in Ref. (author?)<sup>2</sup>, which suggests that the  $\text{O}^*$  intermediate on the  $\text{LaCrO}_3$  surface is not sufficiently destabilized and the ORR kinetics are limited by the rate of surface  $\text{OH}^*$  regeneration. However, using both the GGA+ $U$  method and HSE06 functional we find the relative free energy of  $\text{O}^*$  intermediate becomes about 0.6 eV higher with respect to the GGA result, which makes the  $\text{HO}^*$  regeneration step no longer the most endothermic step in the ORR. Instead, the  $\text{HO}^*/\text{OO}^*$  exchange step (step 1) becomes the potential-determining step. For the HSE06 functional the calculated ORR overpotential is 0.80 V, which is 0.12 V larger than that of  $\text{LaMnO}_3$  but 0.17 V smaller than that of  $\text{LaFeO}_3$ . The overpotential of 0.51 V calculated from the GGA+ $U$  method is much lower than that of  $\text{LaMnO}_3$  (0.76 V) or  $\text{LaFeO}_3$  (0.69 V), in conflict with the experimental observations in Ref. (author?)<sup>2</sup>. We therefore conclude that the GGA+ $U$  method with  $U_{\text{eff}}$  applied on the Cr  $d$  state of  $\text{LaCrO}_3$  may not be a physically appropriate approach to calculate the surface reaction energies.

## Summary

In summary, we conduct a comparative first-principles study of the ORR activity of the three perovskite oxides  $\text{LaMnO}_3$ ,  $\text{LaFeO}_3$  and  $\text{LaCrO}_3$ . In addition to the extensively used GGA and GGA+ $U$  methodologies, we also apply the advanced hybrid-functional method. We find that the calculated surface binding energies of ORR intermediates are strongly dependent on the method, and the free energy diagrams of ORR are described quite differently in GGA, GGA+ $U$  and hybrid functional approaches, especially for  $\text{LaFeO}_3$  and  $\text{LaCrO}_3$  surfaces.

We show that Cr-sites on the  $\text{LaCrO}_3$  surface are better adsorption centers for atomic oxygen than the other two transition metals, but the strong binding of the  $\text{O}^*$  intermediate does not favor the surface hydroxide ( $\text{OH}^*$ ) regeneration step of the ORR process. For the  $\text{LaFeO}_3$  surface the interactions between the Fe-site and the  $\text{OO}^*$  and  $\text{HOO}^*$  intermediates are relatively weak, and the calculated ORR free energy diagram indicates that the  $\text{HOO}^*$  formation and  $\text{OO}^*/\text{HO}^*$  displacement reactions are the primary and secondary potential-determining steps, respectively. These findings agree well with much of the  $e_g$ -filling model deduced from experiments. The results calculated from the hybrid-functional method suggest that the order of ORR activity is  $\text{LaMnO}_3 > \text{LaCrO}_3 > \text{LaFeO}_3$ . This is in better agreement with recent experimental observation in Ref. (author?)<sup>2</sup> than those from the GGA or GGA+ $U$  method. The GGA results yields similar free energy diagrams and ORR activities for  $\text{LaMnO}_3$  and  $\text{LaFeO}_3$ , while the GGA+ $U$  suggest that  $\text{LaCrO}_3$  has the lowest ORR overpotential. In neither case does the obtained order of ORR activity agree with the experiment.

## Acknowledgement

This work was supported by the NSF under Grant No. DMR-0804407. The authors acknowledge DOE/NERSC and UF-HPC centers for providing computational resources. Figures with geometry are produced by VESTA graphical program.<sup>26</sup>



## References

- (1) J. Suntivich, H. A. Gasteiger, N. Yabuuchi, Y. Shao-horn, *J. Electrochem. Soc.* **157**, B1263 (2010)
- (2) J. Suntivich, H. A. Gasteiger, N. Yabuuchi, H. Nakanishi, J. B. Goodenough, Y. S. Horn, *Nature Chemistry* **3**, 546-550 (2011).
- (3) Y. Choi, D. S. Mebane, M. C. Lin, and M. Liu, *Chem. Mater.* **19** 1690-1699, (2007).
- (4) E. A. Kotomin, Y. A. Mastrikov, E. Heifetsa, and J. Maiera, *Phys. Chem. Chem. Phys.* **10**, 4644-4649 (2008).
- (5) Y. Choi, M. E. Lynch, M. C. Lin, and M. Liu, *J. Phys. Chem. C* **113** 7290-7297, (2009).
- (6) A. Kushima, S. Yip, and B. Yildiz, *Phys. Rev. B* **82**, 115435 (2010).
- (7) H.-T. Chen, P. Raghunath, and M. C. Lin, *Langmuir* **27**, 6787-6793 (2011).
- (8) Y.-L. Lee, J. Kleis, J. Rossmeisl, and D. Morgan, *Phys. Rev. B* **80**, 224101 (2009).
- (9) Y.-L. Lee, J. Kleis, J. Rossmeisl, Y. Shao-Horn and D. Morgan, *Energy Environ. Sci.* **4**, 3966 (2009).
- (10) V. I. Anisimov, J. Zaanen, and O. K. Andersen, *Phys. Rev. B* **44**, 943 (1991).
- (11) A. I. Liechtenstein, V. I. Anisimov, and J. Zaanen, *Phys. Rev. B* **52**, R5467 (1995).
- (12) J. Paier, R. Hirschl, M. Marsman, and G. Kresse, *J. Chem. Phys.* **122**, 234102 (2005).
- (13) E. R. Batista, J. Heyd, R. G. Hennig, B. P. Uberuaga, R. L. Martin, G. E. Scuseria, C. J. Umrigar, and J. W. Wilkins, *Phys. Rev. B* **74**, 121102(R) (2006).
- (14) M. Marsman, J. Paier, A. Stroppa and G. Kresse, *J. Phys. Condens. Matter* **20**, 064201 (2008).
- (15) G. Kresse and J. Furthmüller, *Comput. Mat. Sci.* **6**, 15 (1996).

- (16) J. P. Perdew, K. Burke, and M. Ernzerhof, Phys. Rev. Lett. **77**, 3865 (1996).
- (17) S. L. Dudarev, G. A. Botton, S. Y. Savrasov, C. J. Humphreys, and A. P. Sutton, Phys. Rev. B **57**, 1505 (1998).
- (18) L. Wang, T. Maxisch, and G. Ceder, Phys. Rev. B **73**, 195107 (2006).
- (19) J. Heyd, G. E. Scuseria, and M. Ernzerhof, J. Chem. Phys. **124**, 219906 (2006).
- (20) H. J. Monkhorst and J. D. Pack, Phys. Rev. B **13**, 5188 (1976).
- (21) J. K. Nørskov, J. Rossmeisl, A. Logadottir, L. Lindqvist, J.R. Kitchin, T. Bligaard, and H. Jónsson, J. Phys. Chem. B **108**, 17886 (2004).
- (22) Y. Sha, T. H. Yu, Y. Liu, B. V. Merinov and W. A. Goddard III, J. Phys. Chem. Lett., **1**, 856-861(2010).
- (23) G. Henkelman, A. Arnaldsson, and H. Jónsson, Comput. Mater. Sci. **36**, 254-360 (2006).
- (24) I. C. Man, H.-Y. Su, F. Calle-Vallejo, H. A. Hansen, J. I. Martínez, N. G. Inoglu, J. Kitchin, T. F. Jaramillo, J. K. Nørskov, and J. Rossmeisl, ChemCatChem **3**, 1159 (2011).
- (25) H. A. Hansen, J. Rossmeisl and J. K. Nørskov, Phys. Chem. Chem. Phys. **10**, 3722-3730 (2008).
- (26) K. Momma and F. Izumi, J. Appl. Crystallogr. **44**, 1272 (2011).